Experimental investigation of the behavior of UHPCFST under repeated axial tension

Chunlei Yu[a], Min Yu[a], Lihua Xu [a], Yinjie Yang [a], Jianqiao Ye[b]

[a] School of Civil Engineering, Wuhan University, Wuhan 430072, China

[b] School of Engineering, Lancaster University, Lancaster LA1 4YR. UK

Abstract: A ultra-high performance concrete filled steel tube (UHPCFST) is a composite structural component that extends the performance of both steel and concrete. It is a promising component to be used in a diagrid structure to further reduce self-weight. Compared with the research on compressive performance of UHPCFST, there is a lack of knowledge on the mechanical behavior of UHPCFST under axial tension. This paper fills this knowledge gap by carrying out experiments on UHPCFST subjected to monotonic and repeated tension. The test parameters are steel tube thickness and volume fraction of ultra-high performance concrete (UHPC). The failure modes, load-strain curves, tensile strength and tensile stiffness are studied in detail. Stiffness degradation is also studied. The test results show that: (1) under axial tension load, a UHPCFST typically experiences fracture failure of the outer steel tube, followed by section fracture of the UHPC, and notable deformation before a final ductile failure; (2) tensile strength increases with the increase of the thickness of the steel tube, while it is less obvious in a UHPCFST with a higher steel ratio; (3) the force-strain curve of a UHPCFST under monotonical axial tension is close to that of the UHPCFST under repeated axial tension, suggesting that the accumulated damage during unloading and reloading is limited. An exponential decay formula is proposed to predict stiffness degradation observed in the repeated axial tensile tests. It is found that the design codes from Europe, USA, and China underestimate tensile strength and stiffness of UHPCFST. Finally, a three-phase empirical model is proposed for the load-strain curve of UHPCFST under tension.

Keywords: Ultra-high performance concrete (UHPC), Ultra-high performance concrete filled steel tube (UHPCFST), Axial tension, Repeated loading, Load-strain curve.

1. Introduction

A concrete-filled steel tube (CFST) is a composite structure that consists of a steel tube filled with concrete. CFSTs have been used widely in structural engineering due to their high strength, stiffness, and ductility. The combination of steel and concrete in a CFST provides confinement to the concrete, thus enhancing its compressive strength and ductility. CFSTs are widely used in various applications, including bridge piers, columns, and offshore structures. Although the mechanical properties of concrete are improved in the form of CFSTs, the requirement for a large section due to the low strength of normal concrete may lead to increased structural weight, reduced spacing, constructional complexity, and potential aesthetic issues. Replacing normal concrete (NC) with ultra-high performance concrete (UHPC) in CFSTs is one of the options that may overcome the above problems. Compared to normal concrete, high strength concrete and high performance concrete[1,2], UHPC is an emerging high-performance building material that exhibits a series of significant advantages, such as ultra-high compressive strength and exceptional durability[3]. Structures made of UHPC can be up to 1/2 lighter than the same structure made of normal concrete[4], though UHPC is more brittle than NC, *i.e.*, UHPC has reduced deformability and energy absorbability before failure[5]. By replacing NC with UHPC in a CFST, the resulting ultra-high-performance concrete filled steel tube (UHPCFST) can sustain higher loads and exhibit improved mechanical properties. Additionally, the issue of brittleness associated with UHPC can be addressed[6]. Ultra-high-performance concrete-filled steel tubes (UHPCFST) have emerged as a highly promising and innovative composite structural form[7], offering immense potentials for the construction industry.

Recently, diagrid structures with CFST components are increasingly used in, *e.g.*, cooling towers of power plants[8–12] and high-rise buildings[13–16] to increase lateral stiffness of the structures[17]. In a typical earthquake resistance design, diagrid structures can transfer transverse forces to axial forces carried by CFST components. As a result, the CFST components are likely subjected to repeated tensile forces, which is not an idea loading scenario for the CFST as the tensile strength of CFST is relatively low due to the poor tensile properties of the concrete. This hinders the application of CFST when significant tensile loading is present. To the authors' best knowledge, the research on this aspect is relatively rare. Pan[18] analyzed tensile performance of CFST using the theory of elastic-plastic mechanics, alongside a series of axial tensile tests on CFST of different steel tube thickness. It was found that due to the interaction with the concrete, the steel tube yielded at a stress that was up to 10% higher than the yield strength of the steel under uniaxial tension. It was concluded also that the increase of the yield stress depended mainly on the steel ratio of the CFST. To be more specific, Han[19] conducted axial tensile tests on CFST of different steel ratios. It was observed that the increase in the tensile strength of the steel tube decreases linearly with the increase of steel ratio. A formula was then proposed to calculate the tensile strength of the CFST with consideration of tensile strength of concrete. From the research on CFST subjected to tension, including the above, the CFST design codes of Europe, USA and China have all considered tension in practical design.

To increase the tensile strength of concrete, fiber-reinforced concrete (FRC) is used in CFST that, is called Fiber Reinforced Concrete Filled Steel Tubes (FRCFST). It has been observed that FRCFST shows superior tensile properties in comparison with CFST. Xu[20] theoretical analyzed failure of FRCFST and proposed formulas for calculating tensile strength and stiffness by considering three different enhancement effects. The formulas showed good agreement with the experiment results of Han[19] and Pan and Zhang[18]. Due to the fiber reinforcement and close-packing, Reactive Powder Concrete (RPC) exhibits even better mechanical performance than Fiber Reinforced Concrete (FRC). Lai[21] carried out axial tensile tests of RPCFT, and an empirical design equation was proposed to calculate the tensile strength of RPCFT. Alongside the continuous advancement of concrete materials, Ultra-High Performance Concrete (UHPC) has gained significant attention[22,23] as an alternative to RPC due to its exceptional strength and durability. To further enhance the mechanical performance, the use of UHPC results in further space-saving and reduction in self-weight. As a promising replacement of CFST[24], UHPCFST subjected to repeated tensile loading has become an important design issue. However, the research on tensile mechanical performance of UHPCFST is currently rare. To promote future applications of UHPCFST, studies on the mechanical performance of UHPCFST under repeated tensile load are urgently required.

This paper experimentally investigates tensile performance of UHPCFST to fill the gap mentioned above. Eighteen specimens are tested under monotonic and repeated tensile loading to study the tensile performance of UHPCFST. Failure modes, tensile strength, tensile stiffness and tensile stiffness degradation of the UHPCFST are investigated in detail. Existing code provisions and research formulas for calculating the capacity of tensile strength and tensile stiffness are evaluated in this study. An exponential decay formula and a three-phase mathematical model are proposed, respectively, to predict tensile stiffness degradation and to describe the strain-force relationship of UHPCFST subjected to tension.

2. Experimental program

2.1. Specimen design

Eighteen UHPCFST specimens are tested to investigate the mechanical behavior of the UHPCFST subjected to tension. Three groups of UHPCFST, each of which contains a different volume fraction of coarse aggregate, and with three different thicknesses of the steel tube are used to fabricate the UHPCFST specimens for the tensile experiments. To investigate tensile stiffness degradation of the UHPCFST under tensile loading, the specimens are divided into two groups of the same size, *i.e.*, nine of the specimens are for monotonic tension test and the other nine are for repeated tension test. The design details of the eighteen specimens are shown in Table.1. Considering the tensile capacity of load machine and available geometric specifications of the seamless steel tubes in the market, the outer diameter of all the specimens is selected as 108mm. Three different steel thickness, *i.e.*, 4mm, 6mm and 8mm, are considered to evaluate the effect of steel confinement. To mitigate any stability issues, the length of specimen is made three times of the diameter. The coarse aggregate volume fractions are, respectively, 0%, 15% and 30%. The geometric specifications of a typical specimen are shown in Fig.1.

Table.1 Design parameters of specimen

No	Specimen label	D×t× L (mm)	V_{ca} (%)	f_y (MPa)	f_{cu} (MPa)	f_c (MPa)	α	ξ
1	T4CA00-M	108×4×324	0	415	125	101	0.166	0.684
2	T4CA15-M	108×4×324	15	415	134	114	0.166	0.606
3	T4CA30-M	108×4×324	30	415	142	129	0.166	0.535
4	T6CA00-M	108×6×324	00	410	125	101	0.266	1.078
5	T6CA15-M	108×6×324	15	410	134	114	0.266	0.955
6	T6CA30-M	108×6×324	30	410	142	129	0.266	0.844
7	T8CA00-M	108×8×324	0	405	125	101	0.378	1.516
8	T8CA15-M	108×8×324	15	405	134	114	0.378	1.343
9	T8CA30-M	108×8×324	30	405	142	129	0.378	1.187
10	T4CA00-R	108×4×324	0	415	125	101	0.166	0.684
11	T4CA15-R	108×4×324	15	415	134	114	0.166	0.606

12	T4CA30-R	108×4×324	30	415	142	129	0.166	0.535
13	T6CA00-R	108×6×324	0	410	125	101	0.266	1.078
14	T6CA15-R	108×6×324	15	410	134	114	0.266	0.955
15	T6CA30-R	108×6×324	30	410	142	129	0.266	0.844
16	T8CA00-R	108×8×324	0	405	125	101	0.378	1.516
17	T8CA15-R	108×8×324	15	405	134	114	0.378	1.343
18	T8CA30-R	108×8×324	30	405	142	129	0.378	1.187

In Table.1, D, t and L denote, respectively, outside diameter, thickness and length of a steel tube; V_{ca} is coarse aggregate volume fraction of concrete; f_y is yield strength of steel; f_{cu} is cubic compressive strength of UHPC; f_c is cylinder compressive strength of UHPC; α is steel ratio; ξ is [25]confinement factor, and can be computed by $\frac{f_y A_s}{f_c A_c}$. The specimens to be tested are labeled with T*i*CA*jk*-*L*, where Ti denotes thickness of *i*mm, CA*jk* denotes coarse aggregate volume fraction of *jk*% and *L* takes M for monotonic loading and R for repeated loading, respectively.

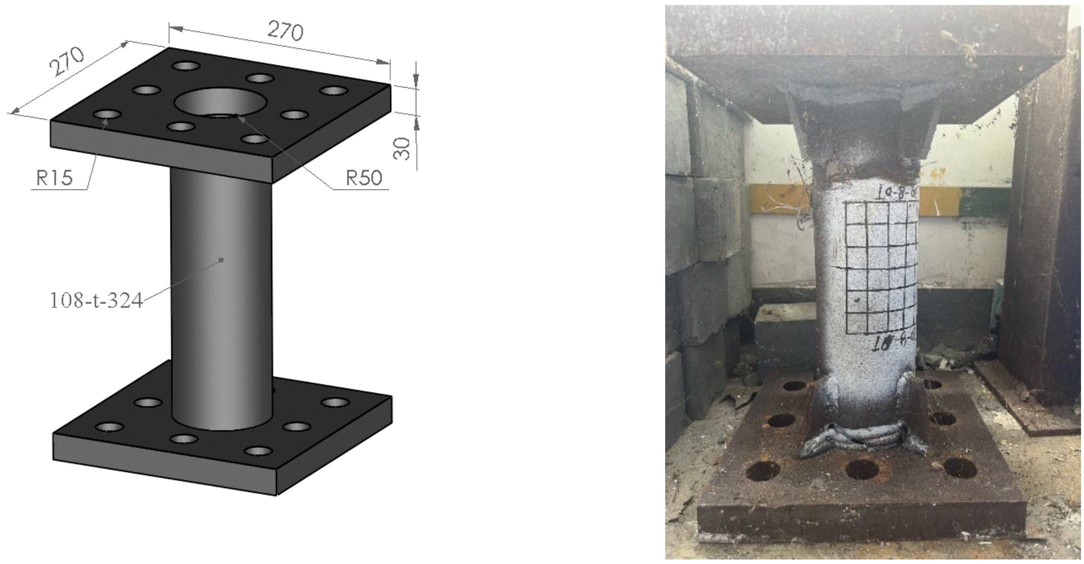

a) Geometry schema of specimen　　　　b) Photograph of specimen

Fig.1. UHPCFST Specimen

2.2. Materials properties

The mechanical properties of a UHPCFST depend on the composite action of the steel tube and the UHPC. Therefore, it is essential to carry out experiments to obtain the basic mechanical properties of these two materials.

2.2.1. Steel

Steel coupons are fabricated from the steel tube according to Chinese code GB/T 228.1:2010[26]. Tensile tests are carried out using the 60T tension-compression quasi-dynamic testing machine, as seen in Fig.2. The applied force is measured by the force sensor of the test machine. A strain gauge is used to record the tensile strain of the test sample. Displacement loading control is applied during the test with a loading rate of 0.5mm/min. The failure modes and stress strain curves of the samples are shown in Fig.2. All the tests show fracture at the center of the specimens as the predominant failure mode. The stress-strain curves all show noticeable yield plateau. Table.2 presents the yield strength, ultimate strength, elastic modulus and Poisson's ratio of the tested samples.

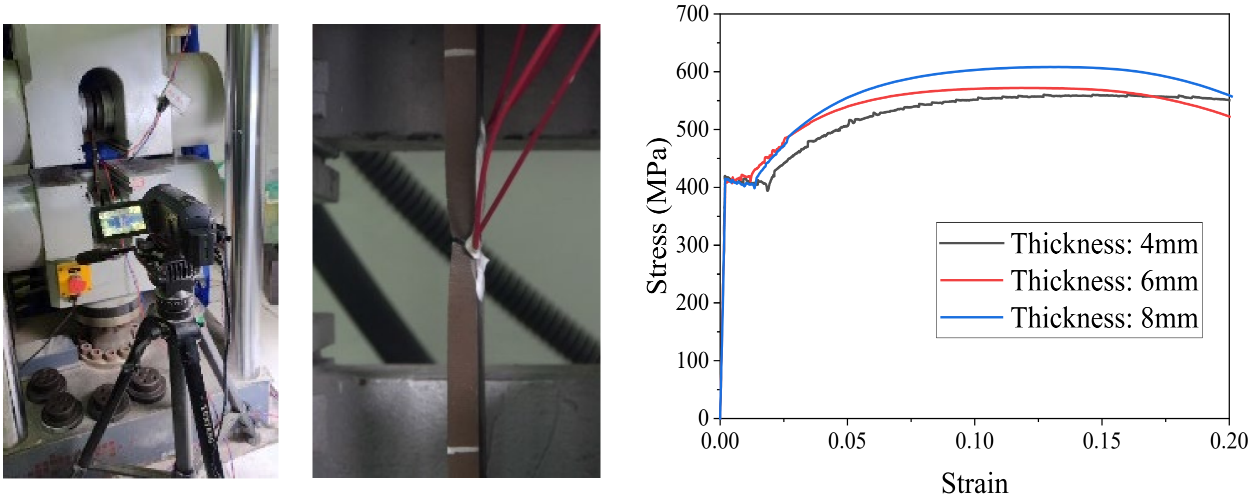

a) In test b) Failure mode c) Strain stress curve

Fig.2. Tensile test of steel tube

Table.2 Properties of steel tube

No	Sample Label	diameter (mm)	Thickness (mm)	Yield stress (MPa)	Ultimate stress (MPa)	Elastic module (GPa)	Poisson's ratio
1	S1	108	4	415	560	210	0.30
2	S2	108	6	412	570	196	0.28
3	S3	108	8	406	610	199	0.29

2.2.2. Ultra-high performance concrete (UHPC)

Three mixtures of ultra-high-performance concrete are tested to investigate the effect of coarse aggregate volume fraction on the tensile properties of the UHPC. The details of the mixtures are shown in Table.3. P.O.52.5 cement, silica fume with 95 % Si content and fly ash are used as binder of the concrete. Polypropylene fibers of 18-48 μm in diameter and straight copper coated steel fibers of 13 mm in length and 0.2 mm in diameter are added to the mixture. To improve the fluidity of the fresh mixture, highly effective polycarboxylate superplasticizer powders are used. Quartz sand with particle size of 69-178 μm and basalt of 5-10 mm are the respective fine and coarse aggregate of the UHPC. Based on the Chinese Standard[27] and previous research[28,29]. 0%, 15% and 30% coarse aggregate volume fractions, i.e., CA00, CA15 and CA30, are chosen to ensure both strength and workability of the UHPC. To ensure an even distribution of the polypropylene and steel fibers, ultrasonic waves are utilized to disperse the polypropylene in water. The steel fibers are added into the working mix machine through bucket shaking.

Table.3 Mixture of UHPC

Mixture (kg/m^3)	Cement	Silica fume	Fly ash	Water	Quartz sand	Coarse Aggregate	Super plasticizer	Steel fiber	Polypropylene fiber
UHPC-CA00	857	107	107	182	1179	-	11.8	157 (2%)	1.9 (0.2%)
UHPC-CA15	725	91	91	154	998	375 (15%)	10	157 (2%)	1.9 (0.2%)
UHPC-CA30	594	74	74	126	817	750 (30%)	8.2	157 (2%)	1.9 (0.2%)

According to the Chinese Code T/CCPA 35—2022[30], cubic samples (100mm×100mm×100mm) are fabricated to measure cube compressive strength of the UHPC, and cylinder samples (100mm×200mm) are made to measure cylinder compressive strength and Elastic module of the UHPC. The cubic compressive strength of the three types of UHPC all exceeds 120 MPa, meeting the cubic compressive strength requirement specified in the a Chinese industry standard code[31]. The measured mechanical properties are shown in Table.4. From Table.4, it is evident that the compressive strength and elastic modulus change as the coarse aggregate content in the mixture changes. In addition to the compressive mechanical performance of the UHPC, previous research conducted by Xu[32] also investigated tensile properties of the same UHPC. Furthermore, a formula for the tensile strength of the UHPC was proposed.

Table.4 Mechanical Properties of UHPC

UHPC	Cube compressive strength (MPa)	Cylinder compressive strength (MPa)	Elastic module (GPa)
UHPC-CA00	126	101	47
UHPC-CA15	135	114	48
UHPC-CA30	143	129	51

2.3. Test set-up and load patterns

The tensile experiments of the UHPCFST are carried out on a servo-hydraulic material test system (MTS) that has a 250-tone tensile/compressive load capacity in the laboratory of Structural Engineering, Wuhan University. There are 12 bolts distributed on the loading plate of the MTS to apply tensile load to the specimen. Two tensile transfer plates are designed to connect the end-plates of the specimen to the MTS loading plates at the top and bottom of the specimen to prevent buckling of the end-plates and reduce steel usage, as shown in Fig.3.

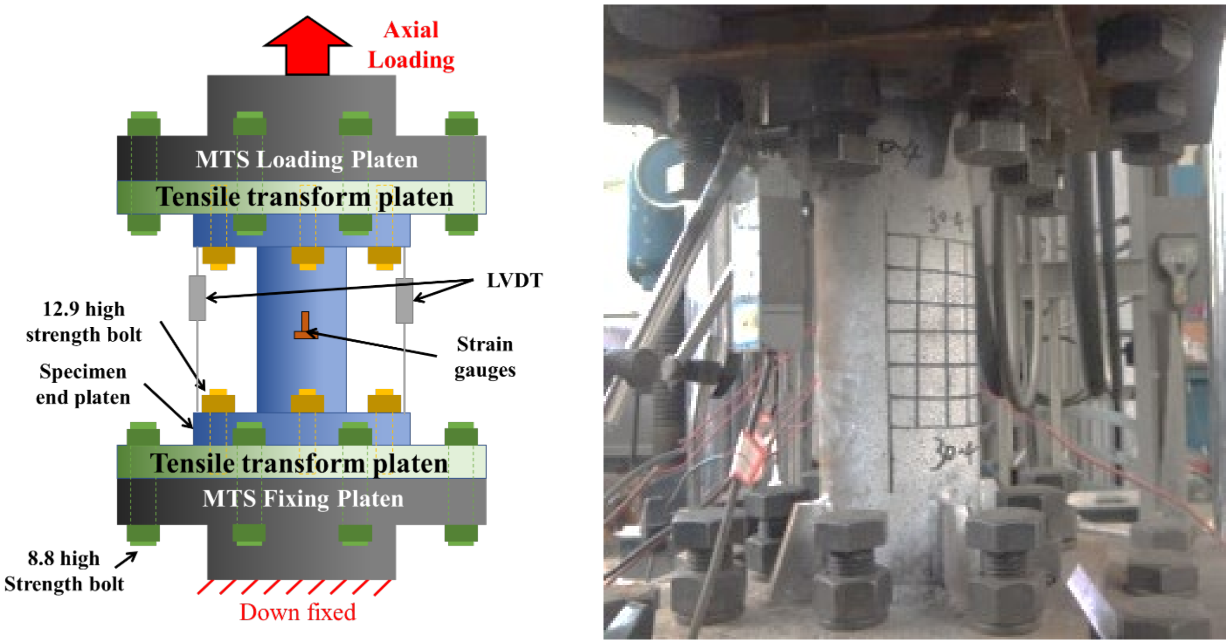

a) schematic diagram

b) Photo of the test

Fig.3. Test set-up

To set up the test, the two tensile transfer plates are connected first to the MTS loading plates by grade 8.8 high strength bolts. The endplates of the specimen are then screwed to the transfer plates using grade 12.9 headed screws. Two linear variable differential transformers (LVDTs) are mounted vertically to capture the axial displacement of the specimen. Prior to conducting the specimen test, to ensure a uniform distribution of the load on the specimen plate, a pre-load stage is implemented. The plates are adjusted using bolts until the measurements of the two LVDTs are sufficiently close.

Two different loading patterns (monotonic tension and repeated tension) are applied in the experiments, as shown in Fig.4. Displacement-controlled loading with variable loading rates is selected, as seen in Fig.4a. For monotonic tension, a constant loading rate of 1mm/min is applied until final fracture of the specimen. For the repeated tension tests, a loading rate of 1 mm/min and 1.5 mm displacement increment per loading cycle are applied before 6 mm displacement is reached. The loading rate and displacement increment per loading cycle are increased to 2mm/min and 3 mm respectively until failure of the specimen.

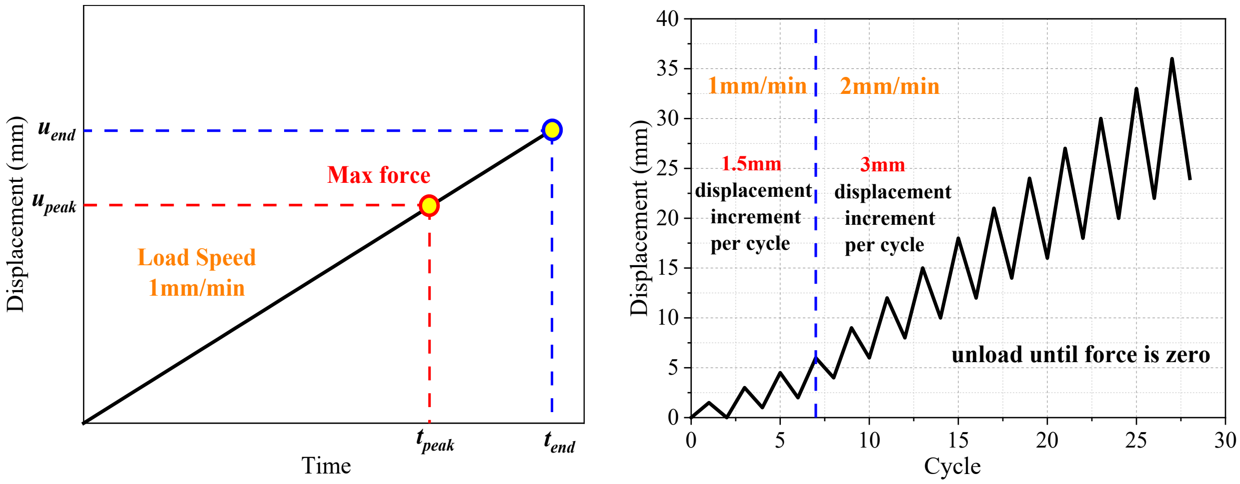

a) Monotonic tensile experiments

b) Repeated tensile experiments

Fig.4. Displacement controlled load patterns

3. Test results and analysis

3.1. Failure modes

Fig.5 presents the final failure modes of the UHPCFST, where the maximum tensile load and the cracks of each of the UHPCFST are shown. The maximum tensile load increases with the increase of the steel tube thickness due to the increased steel sectional area. The maximum tensile load of the specimens under repeated tensile load is slightly smaller than that of the corresponding specimen under monotonic tensile load. It can be attributed to the effect of the extra damage produced by the loading and unloading process. Fracture occurs at around 1/3 height of all the specimens. Notably, the profile of the fracture varies depending on the thickness of the steel tube and the load pattern. The specimen with a thicker steel tube exhibits a wider and flatter fracture pattern. As the steel tube thickness increases, the bonding between the concrete and the steel tube is strengthened[33]. Consequently, the force transferred from the steel tube to the concrete is higher and more uniformly distributed, leading to a wider and flatter fracture pattern. Furthermore, The UHPCFST, T8CA15-M, subjected to monotonic tension shows smaller fracture width than that of the same UHPCFST under repeated tension. This discrepancy can be attributed to the additional damage incurred during the unload and reload processes. Upon removing the specimens from the test rig, it was observed that, in most cases, the UHPC was also fractured at around 1/3 height of specimens, leading to complete splitting of the specimens.

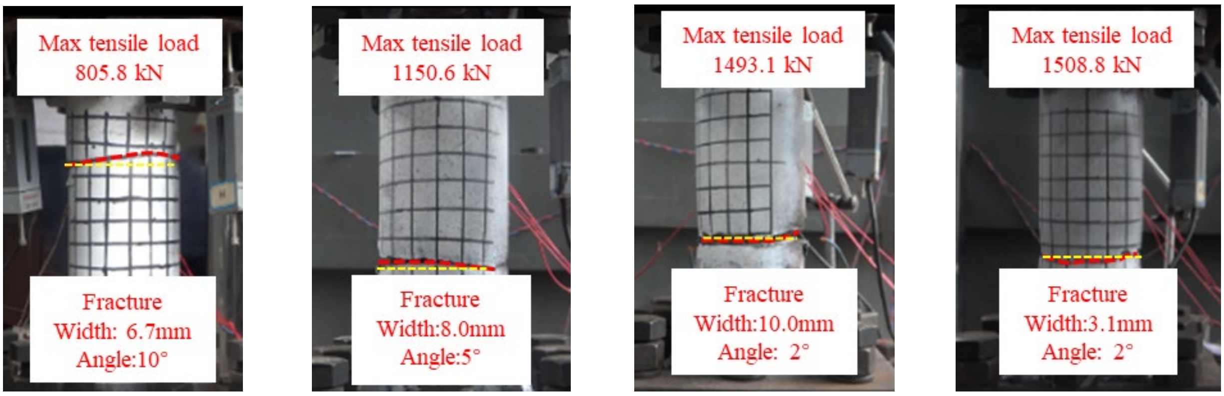

T4CA15-R T6CA15-R T8CA15-R T8CA15-M

Fig.5. Failure modes of UHPCFST under tensile load

3.2. Load versus strain curve

The tensile load (N_t) of the specimens is plotted in Fig.6 against the longitudinal strain (ε). The tensile load (N_t) is recorded by the test machine, while the longitudinal strain (ε) is determined by dividing the average LVDT measurements by the specimen height. The N_t-ε curves of all the tested CFST specimens show similar characteristics. For the specimens under monotonic tension, initially, the curves show an approximately linear phase until the steel tubes yield, which are followed by an elastic-plastic stage, and then a "strain harden" stage until failure. With further increase of steel strain, the steel tubes contract significantly in the radial direction. Noticeable necking of the specimens is observed before fracture and the final tensile failure of the specimens. For a given specimen subjected to repeated tension, the unloading and reloading stiffness of the specimen are slightly smaller if the unloading or reloading starts from a higher strain during the loading process. Careful observation of

Fig.6 shows that the reduction in the loading stiffness is less obvious when the steel tube is thicker, which may be attributable to the reduced concrete damage in the specimen with thicker steel. It can also be seen from Fig.6 that the monotonic loading curves are very close to the load envelopes of the respective repeated tensile loading curves, which suggests that the influence of loading and unloading on the specimens' load-strain curves is relatively minor.

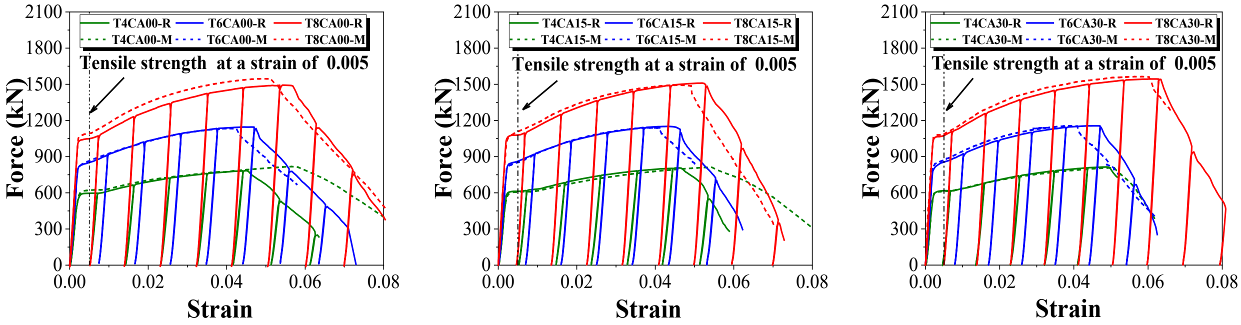

a) CA00 b) CA15 c) CA30

Fig.6. Force strain curve of UHPCFST under tension

Fig.7 shows the typical N_t-ε curve of a UHPCFST under tension. There are five phases during a monotonic loading process, i.e., the linear, nonlinear, plateauing, hardening and fracture phase. In the linear phase, the section elastic module $(EA)_t$ remains relatively constant, and the N_t-ε curve maintains linear until the stress in the steel tube reaches its elastic proportional limit, where the force reaches N_e, and the strain reaches the linear elastic limit strain (ε_e). In the nonlinear phase, the steel tube begins to exhibit nonlinear properties with gradual reduction of the section module $(EA)_t$. When the tensile force reaches the tensile strength (N_{0t}), the strain reaches the yield strain (ε_y). As the displacement-controlled load continues to increase, the curve comes to the plateauing phase, in which the deformation of the steel tube continues to increase, while the force in the steel remains almost constant. The continuous yielding of the steel tube creates increased contact interaction between the tube and the UHPC. This may result in further development of the initial cracks in the UHPC and the occurrence of additional sub-cracks. In the hardening phase, the strain is larger than the hardening strain limit (ε_h), and the force increases with the increase of the plastic deformation at a rate that is much smaller than that of the elastic phase. Steel tube starts necking and the interaction between the steel tube and the UHPC increases, resulting in propagation of the existing cracks. In the fracture phase, the steel tube starts fracturing, and the main crack of the UHPC may have spanned over the entire section, resulting in the final failure of the specimen. For repeated tensile loading, the load-strain curves of unloading and reloading are nearly identical and linear. The current section modulus, $(EA)_t^*$, is lower than the initial section modulus $(EA)_t$, as a result of the accumulated damage in the UHPC and the steel.

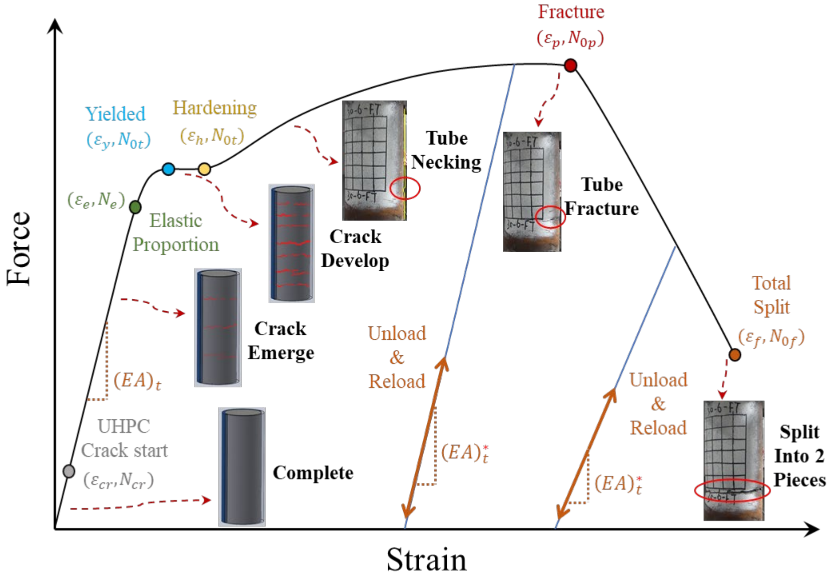

Fig.7. Force-strain curve of UHPCFST under axial tension

3.3. Analysis of result

3.3.1. Tensile strength

In this paper, tensile strength (N_{0t}) of the UHPCFST subjected to tension is defined as the tensile load at a longitudinal tensile strain of 5000 $\mu\varepsilon$. The reasons for this definition are as follows. When the longitudinal tensile strain reaches 5000 $\mu\varepsilon$, the steel tube has already yielded, and the tensile load versus longitudinal strain curve has nearly completed its elastic stage. The tensile strain tends to develop significantly, while the corresponding increase in tensile load is relatively slow, as shown in Fig.6. Using the above defined tensile strength, the measured tensile strengths of the UHPCFST specimens are presented in Fig.8.

Fig.8 shows the tensile strength of the UHPCFST specimens with different steel tube thickness and volume fraction of coarse aggregate in the UHPC. For both monotonically and repeatedly loaded, an increase in the thickness of the steel tube always results in a significant increase in the tensile strength of the UHPCFST. However, a conclusive statement cannot be made on the effect of volume fraction of coarse aggregate in the UHPC on the tensile strength. The ratios between the tensile strength of the monotonically and the repeatedly loaded specimens are shown in Fig.8 c), which is close to one. This observation implies that the unloading and reloading process have little effect on the tensile strength.

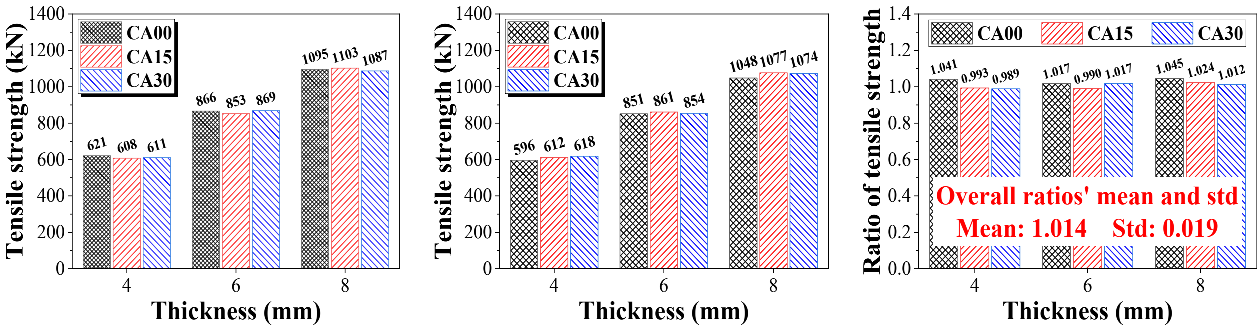

a) Monotonic loading | b) Repeated loading | c) Comparison between monotonic and repeated loading

Fig.8. Tensile strength of the test specimens

To investigate the factors that affect tensile strength of a UHPCFST, a tensile strength factor (k_t) is introduced and defined in Eq.(1), where N_{0t} is tensile strength of UHPCFST, f_y is yield strength of steel tube and A_s is sectional area of steel tube.

$$k_t = \frac{N_{0t}}{f_y A_s} \tag{1}$$

Fig.9 shows the relationship between the tensile strength factor (k_t) and the confinement factor

(ξ), steel ratio (α) and tensile strength of UHPC (f_t). It is worthy of noting that the tensile strength of UHPC (f_t) with different volume fraction of coarse aggregate is calculated by Eqs.(2), which were proposed by Xu[32].

$$f_t = 5.523(1 + 0.523\alpha_{sf} - 0.643\alpha_{CA}) \\ \alpha_{sf} = \rho_{sf}\lambda_{sf} \qquad \alpha_{CA} = \rho_{CA} \tag{2}$$

where ρ_{sf} and λ_{sf} are fraction volume and aspect ratio of steel fiber of the UHPC matrix, respectively, α_{CA} is fraction volume of coarse aggregate of UHPC matrix. In Fig.9, it can be seen that as the confinement factor increases, the tensile strength factor decreases, except the CA15-M specimen series, of which the tensile strength factor of specimen T8CA15-M is greater than that of specimen T6CA15-M. This is attributable to the lack of yielding of T8CA15-M after the linear phase, thus the force continues to increase with the increase of strain, resulting in the elevated tensile strength at a strain of 0.005. The similar tendency applies also to the steel ratio. The effect of tensile strength of the UHPC on the tensile strength factor is not clear. For all the test specimens, the strength factors are always greater than one, indicating that there is significant enhancement effect for steel tube due to the UHPC.

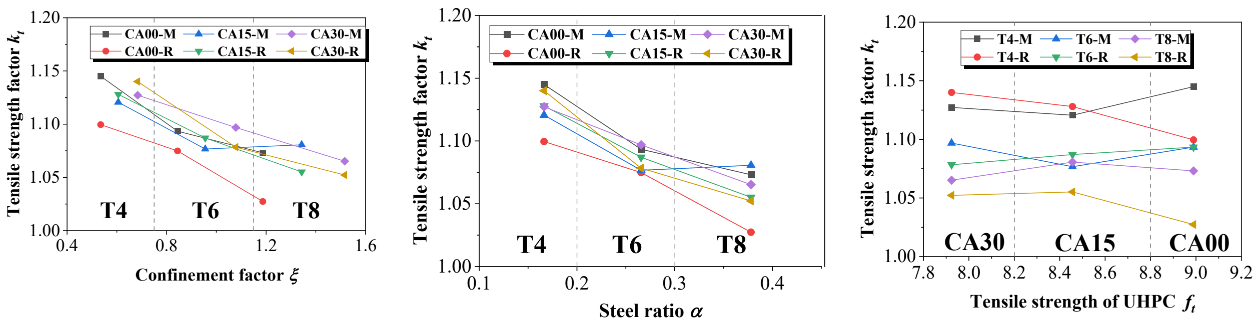

Fig.9. The relationship between tensile strength factor (k_t) and selected factors

3.3.2. Tensile stiffness

To determine the stiffness of the UHPCFST, a calculation method is proposed below. Fig.10 presents a typical unloading and reloading cycle, on which the tangent stiffness of the unloading and reloading paths is also calculated and shown. As seen from Fig.10, fluctuation and significant change of the stiffness occur in the region where the loading is about changing direction, at which the stiffness may be significantly lower due to plasticity or changes in the contacts between different material components. Thus, for consistency, only the middle 60% of the unloading and reloading path are used to calculate the tangent stiffness, i.e., in the range of 0.2P to 0.8P, where P is the tensile force at which unloading starts. The linear regression method is used to establish a linear relationship between the force and the strain within the middle 60% of the data, from which the stiffness of the specimen can be determined. For calculating the initial stiffness, P is replaced by the force at yielding.

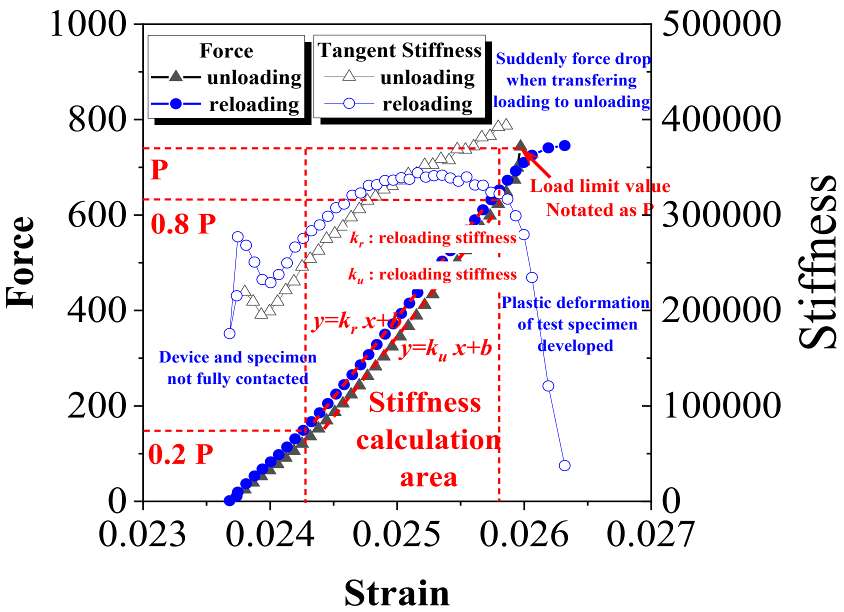

Fig.10. Stiffness calculation point selection and method in reloading and unloading process.

This paper considers three stiffness, i.e., initial stiffness, unloading stiffness, and reloading stiffness. For both monotonic and repeated loading, the initial stiffness is calculated from the ascending curve prior to yielding. The unloading and reloading stiffness only applies to the repeated loading paths. The effect of the design variables of the specimen on the initial tensile stiffness is similar to that on the tensile strength, as shown in Fig.8 and Fig.11. When comparing the initial stiffness of the monotonic specimen with that of the repeatedly loaded specimens, in most cases, the initial stiffness for both loading methods is close.

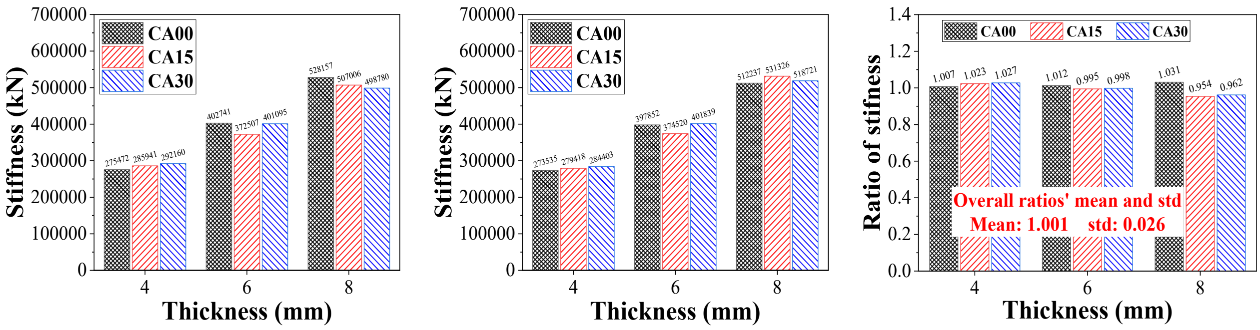

a) Monotonic loading

b) Repeated loading

c) Comparison between monotonic and repeated loading

Fig.11. Initial stiffness of the test UHPCFST specimens

In this section, the analysis is focused on the first pair of unloading and reloading stiffness of all the repeated tensile tests. Fig.12a) presents the first reloading stiffness of all the specimens. For specimens of the same steel thickness, the reloading stiffness is almost the same. The reloading stiffness is slightly smaller than that of the unloading stiffness, as shown in Fig.12b). Fig.12c) shows the ratio between the initial stiffness and the first reloading stiffness. It is evident that the reloading stiffness is slightly greater than the initial stiffness for all the specimens. It is important to note that the ratio between the first reloading stiffness and the initial stiffness decreases with the increase of the tube thickness. The slight increase in the reloading stiffness may be attributable to the fact that some of the contacts between the test machine and the specimens are not fully engaged. To minimize the influence of these factors, the reloading stiffness is considered as the stiffness of the UHPFST in the analyses below.

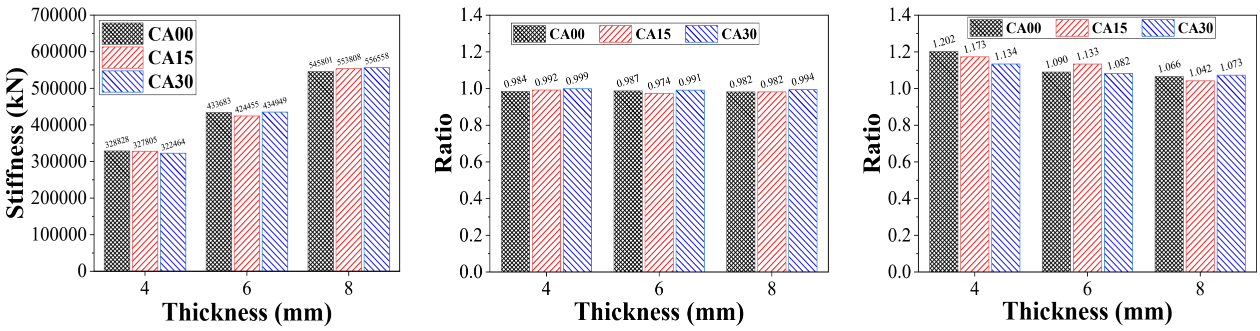

a) Reload stiffness

b) Ratio between reloading

c) Ratio between reloading

stiffness and unloading stiffness stiffness and initial stiffness

Fig.12. Tensile stiffness of specimens under repeated load in the 1st unloading and reloading process

To study the effect of the confinement factor, steel ratio and tensile strength of UHPC on the tensile stiffness of the UHPCFST, a tensile stiffness factor (S_t) is introduced as shown in Equation (3). In this equation, $(EA)_t$ represents section modulus, E_s denotes elastic modulus of the steel tube, and A_s represents sectional area of the steel tube.

$$S_t = \frac{(EA)_t}{E_s A_s} \tag{3}$$

The relationships between the tensile stiffness factor (S_t) and the above factors for the UHPCFST under repeated axial tensile load are presented in Fig.13. Similar to the tensile strength factor (k_t), the tensile stiffness factor decreases as the confinement factor or the steel ratio increases. However, there is not a conclusive observation for the tensile strength of the UHPC. Notably, the tensile stiffness factors are always greater than 1, indicating an increase in the tensile stiffness due to the presence of the UHPC.

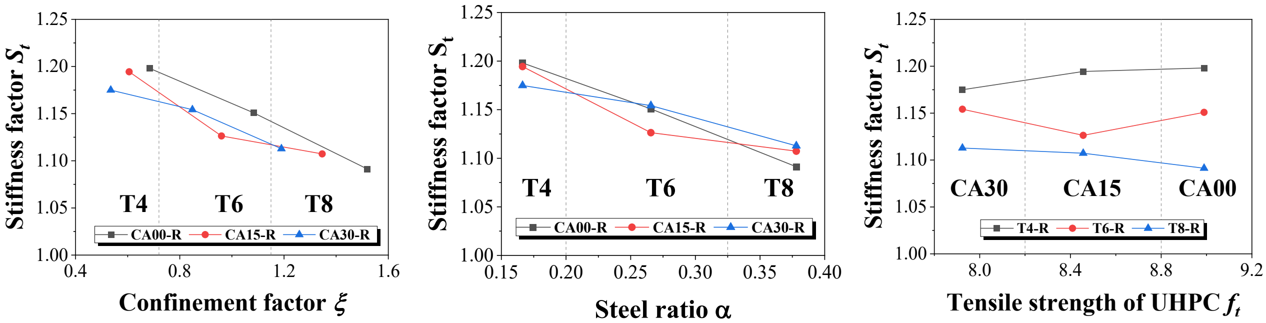

Fig.13. Tensile stiffness factor (S_t)

3.3.3. Stiffness degradation

Damage to the materials of the UHPCFST occurs during the loading process. Macroscopically, this is manifested as a gradual attenuation of stiffness. The degree of stiffness attenuation is crucial for the UHPCFST under seismic load. In the repeated tensile tests, the stiffness of a specimen under a given unloading strain can be calculated, which makes it possible to study stiffness attenuation of the UHPCFST subjected to tension.

Fig.14 illustrates the reloading stiffness for each unloading and reloading process of all the test specimens under repeated tensile load. It can be observed that a thicker steel tube has higher reloading stiffness throughout the entire loading process. The reloading stiffness remains relatively constant before reaching the maximum, but decreases rapidly thereafter.

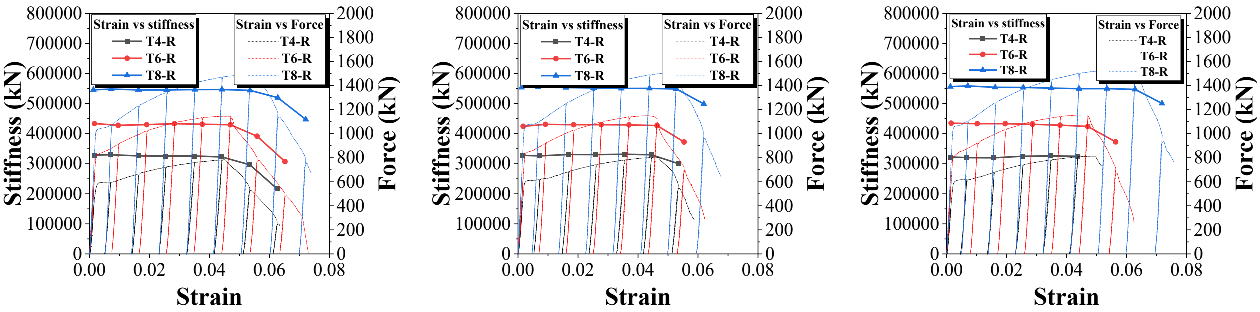

a) CA00 b) CA15 c) CA30

Fig.14. Stiffness degradation for all repeated specimens

To further investigate stiffness degradation in the UHPCFST under tensile load, a stiffness reduction factor (D) is introduced. The factor D can be calculated using Equation (4), where $K_{unloading\{i\}}$ represents the reloading stiffness of the i-th unloading and reloading process.

$$D = K_{unloading\{i\}}/K_{unloading\{1\}} \tag{4}$$

Fig.15 illustrates the relationship between the stiffness reduction factor (D) and the unloading strain for all the repeated tensile specimens.

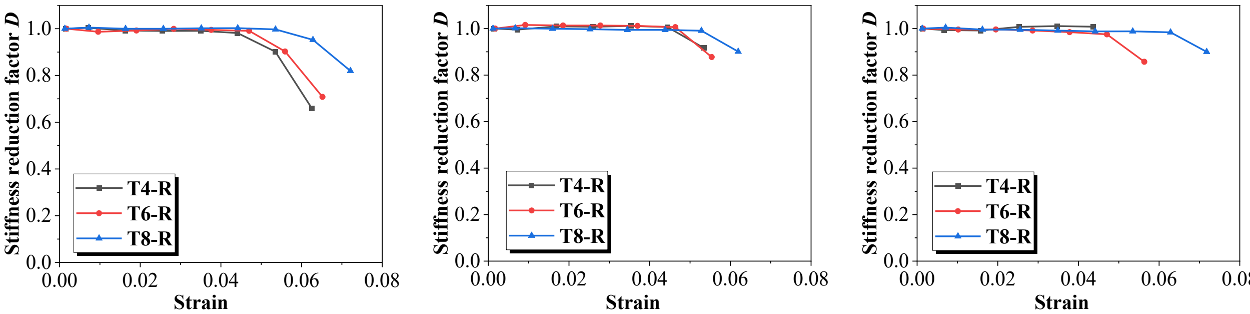

a) CA00 b) CA15 c) CA30

Fig.15. Stiffness reduction factor for all repeated tensile specimens

It can be observed that D follows similar patterns for all specimens. Before the load reaches its peak point, D remains close to 1 consistently. However, once the curve passes the peak point, where specimens start to fracture, D decreases rapidly. Furthermore, it is noticeable that the D of a specimen with thicker steel tube reduces at a lower rate.

4. Calculation of tensile properties of UHPCFST

4.1. Tensile strength

With the increasing applications of CFST, it is essential to evaluate their tensile performance. Many methods for calculating tensile strength have been proposed, as summarized in Table.5.

Table.5 Commonly-used formulas to calculate tensile strength of CFST

Reference	Formulas	Notation
Eurocode 4 AISC 360-16	$N_{0t} = f_y A_s$	Neglect effect of infilled concrete
GB50936-2014	$N_{0t} = 1.1 f_y A_s$	Constant 10% enhancement due to infilled concrete
Han (2011)	$N_{0t} = (1.1 - 0.4\alpha) f_y A_s$	Enhancement factor considering steel ratio due to infilled concrete
Lai (2020)	$N_{0t} = (1.1 - 0.4\alpha) A_s f_y + A_c (0.9 f_t)$	Enhancement of steel section capacity and remain capacity for infilled concrete section
Xu (2017)	$N_{0t} = \alpha_{strength} f_y A_s$ $\alpha_{strength} = \alpha + \beta$ $\alpha = \frac{10.35}{\rho_s^{0.85} + 9.2}$ $\beta = \frac{f_t^*}{f_y \rho_s}$	with hypothesis of thin-wall tube

After comparing the structures of all the formulas in Table.5, the following unified formula, as shown in Eq.(5), is constructed by introducing two parameters, ω_s and ω_c. Thus, each formula in Table.5 can be taken as a special case of Eq.(5) with two specifically defined ω_s and ω_c, as shown in Table.6.

$$N_{0t} = A_s(\omega_s f_y) + A_c(\omega_c f_t) \tag{5}$$

Table.6 Formulas in Table.5 expressed uniformly by Eq.(5)

Reference	ω_s	ω_c
Eurocode 4[34] AISC 360-16[35]	1	0
GB50936-2014[36]	1.1	0
Han (2011)[25]	$1.1-0.4\alpha$	0
Lai (2020)[37]	$1.1-0.4\alpha$	0.9
Xu (2017)[38]	$\frac{10.35}{\alpha^{0.85}+9.2}$	$\frac{f_t^*}{f_t}$

Standard codes of practice in China, Europe, and the United States, namely GB50936, Eurocode 4, and AISC360-16, respectively, provide calculation methods for tensile strength of CFST. Eurocode 4 and AISC 360-16 ignore the contribution from concrete and only consider steel tube in the calculation of tensile strength. GB50936 considers the effect of concrete on preventing inward instability of the steel. As a result, the calculated tensile strength of CFST is about 10% higher.

In addition to the standard codes of practices, many researchers, such as Han, Lai, and Xu, have conducted research on tensile performance of CFST and proposed formulas for calculating tensile strength. Han conducted tensile tests on concrete filled steel tube and found that as the steel ratio increases, the contribution of concrete to the tensile strength of a CFST gradually decreases. Lai conducted experimental research on the tensile performance of fiber-reinforced concrete filled steel tube. The fiber-reinforced concrete has higher tensile strength and also contributes to preventing inward instability of steel tube. Therefore, based on Han's formula, an additional term to include the tensile strength of fiber-reinforced concrete, $A_c(0.9f_t)$, was considered. Xu proposed an analytical model for predicting strength and stiffness of CFST by considering confining effect, fiber-reinforcing effect, and tension-stiffness effect.

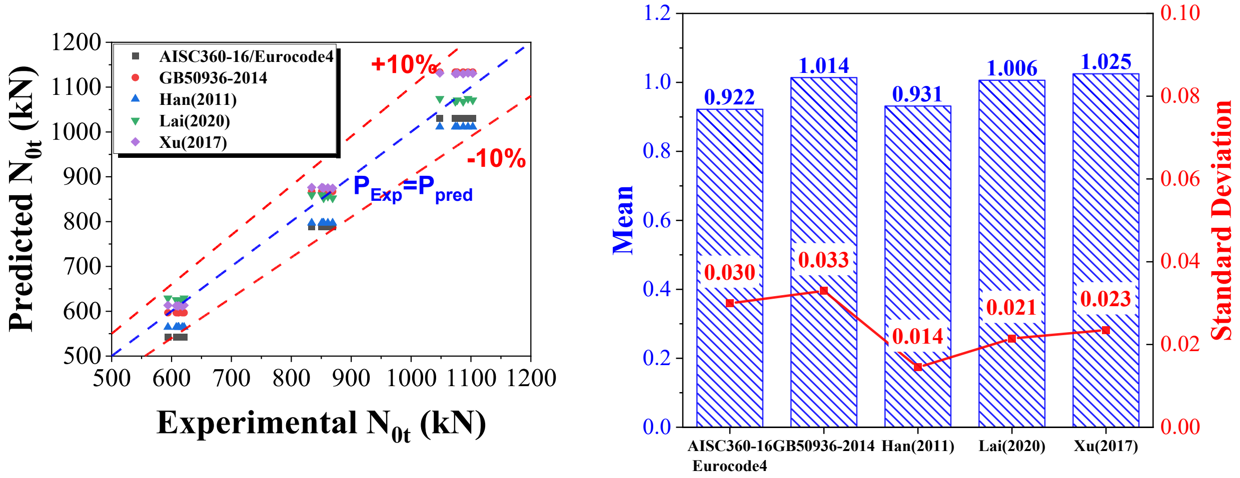

a) P_{Exp} Vs P_{Pred} b) Statistical analysis of P_{Pred}/P_{Exp}

Fig.16. Evaluation of different methods for tensile strength prediction

Using the existing methods, the calculated results of the specimens are presented in Fig.16. AISC360-16 and Eurocode4 apparently underestimate tensile strength of the UHPCFST. GB50936-2014 is more accurate than AISC360-16/Eurocode4. Due to the addition of fibers, the tensile strength of ultra-high performance concrete (UHPC) is significantly enhanced compared to the ordinary concrete. Han's formula does not account for this strengthening effect, leading to an underestimated prediction. Considering the tensile strength of fiber-reinforcement concrete, Lai's formula is the most accurate. The accuracy of the predicted results from the formula proposed by Xu varies with the volume fraction of coarse aggregates of the UHPC. When the volume fraction of coarse aggregate is 0% and 15%, the predictions are accurate. When the volume fraction of coarse aggregate is 30%, the predicted results are overestimated.

4.2. Tensile stiffness

Han and Xu have proposed formulas to calculate tensile stiffness of CFST, as seen in Table.7. The results of using Han and Xu's methods are presented in Fig.17. For UHPCFST, the addition of fibers significantly improves tensile strength of the internal concrete. Han's formula for normal concrete filled steel tube does not take this into consideration, resulting in a smaller stiffness coefficient and thus underestimating the tensile stiffness of UHPCFST. Xu's formula for fiber-reinforced concrete, on the other hand, takes this into account and provides a more accurate prediction.

Table.7 Existed formulas to calculate tensile strength of CFST

Reference	Formulas	Notation
Han (2011)[25]	$(EA)_t = E_s A_s + 0.1 E_c A_c$	Enhancement factor considering steel ratio due to infilled concrete
Xu (2017)[38]	$(EA)_t = \alpha_{stiffness} E_s A_s$ $\boldsymbol{\alpha}_{stiffness} = \left(\frac{1}{1-0.3\psi}\right)\cdot\left(1+\frac{2\beta}{\alpha-\beta}\right)\cdot\left[\frac{0.75\,ln\left(1-\frac{2\gamma}{\alpha-\beta}\right)}{\left(1-\frac{2\gamma}{\alpha-\beta}\right)^{0.75}-1}\right]$ $\psi = \frac{0.3}{1+2.24\rho_s}$	Theory deduction with hypothesis of thin-wall tube

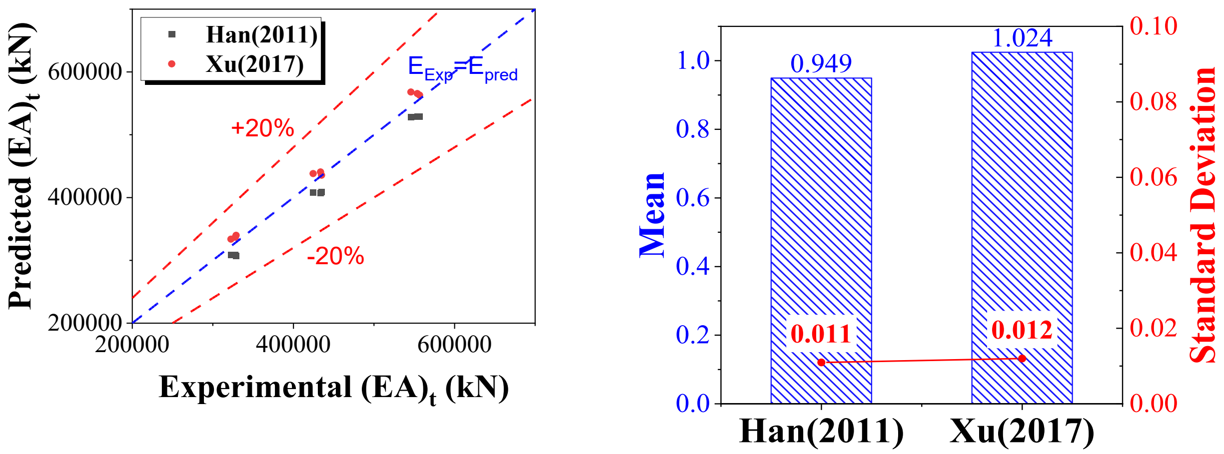

a) E_{Exp} Vs E_{Pred} b) Statistical analysis of E_{Pred}/E_{Exp}

Fig.17. Evaluation of different methods for tensile stiffness prediction

4.3. Stiffness degradation

As mentioned in Section 3.3.3, stiffness reduction factor (D) has been introduced to describe the phenomenon of stiffness degradation of the UHPCFST under axial tension. In practice, Weibull distribution is usually applied to calculate failure possibility of structure. In this paper, the stiffness degradation is regarded as the results of micro-structure failure of the steel tube and UHPC. The cumulative distribution function of Weibull distribution is selected to calculate the stiffness reduction factor. The original cumulative distribution function (CDF) of Weibull distribution is shown in Equation (6). Here the reliability function is defined in Equation (7) to calculate the actual value of the stiffness reduction factor.

$$F(\varepsilon) = 1 - e^{-\left(\frac{\varepsilon}{\eta}\right)^{\beta}} \tag{6}$$

$$D(\varepsilon) = R(\varepsilon) = 1 - F(\varepsilon) = e^{-\left(\frac{\varepsilon}{\eta}\right)^{\beta}} \tag{7}$$

In Equations (6) and (7), ε is longitudinal strain of the UHPCFST, η and β are two parameters that depends on design factors. It was mentioned in Section 3.3.3 that the stiffness degradation varies with the thickness of the steel tube. Fig.18 shows 3 $D-\varepsilon$ curves of the repeated loading tests, i.e., T4CA00-R, T6CA00-R, T8CA00-R, that are used to form the regression formulas of η and β, as shown in Equation (8). In this equation, α is steel ratio of specimen.

$$\eta = \frac{1}{17e^{-\alpha}}, \qquad \beta = 8.6 \tag{8}$$

Fig.18 also shows that the proposed formula can give a relatively accurate prediction to the stiffness reduction factor (D).

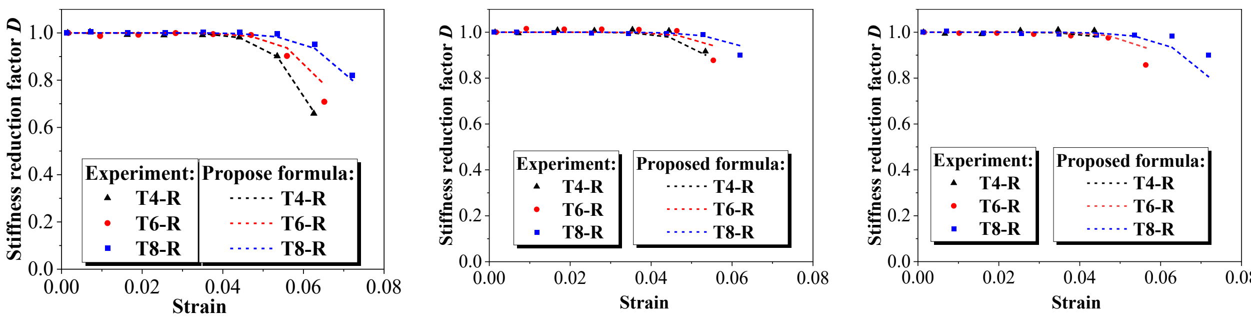

a) CA00 b) CA15 c) CA30

Fig.18. Prediction of proposed formula for stiffness reduction factor

4.4. Proposed model for load-strain curve

The empirical curve for the load-strain response of a UHPCFST under tension is of great importance. It serves as a valuable tool for studying the behavior of the component, predicting its structural response, and optimizing the designs. There are lots of detailed researches about mechanics of CFST, like stress-dependent[39–41], splitting crack[42,43] and micro-cracks[44,45] of confined concrete. In this section, to avoid redundant considerations about possible factors' effect on mechanical behaviour, an empirical load-strain curve is constructed and evaluated for UHPCFST under tension, incorporating elastic, yield, and hardening phases.

4.4.1. Envelope curve

The empirical load-strain curve consists of two parts, i.e., the envelope curve and the unloading & reloading paths. |The envelope curve can describe the mechanical behavior of structural component under a monotonic load. As analyzed in Section 4.4, there are four phases needing to be considered in a typical experimental strain force curve for UHPCFST under monotonic tension, including the linear, nonlinear, plateau, and hardening phases. For the sake of simplicity, the envelope strain-force curve ignores the nonlinear phase. As a result, the following formulas in Eq.(9) are constructed.

$$F = \begin{cases} (EA)_t \varepsilon & \varepsilon < \varepsilon_y \\ N_{0t} & \varepsilon_y < \varepsilon < \varepsilon_h \\ k_1 \varepsilon^2 + k_2 \varepsilon + k_3 & \varepsilon_h < \varepsilon < \varepsilon_u \end{cases} \tag{9}$$

In the elastic phase, a linearly equation is sufficiently accurate, and this phase ends when the strain exceeds the yield strain. The section stiffness and tensile strength in the linear phase can be obtained by the formulas proposed by Xu in Table.5 and Table.6, respectively.

In the phase of yield plateau, the force remains constantly at the tensile strength. This yield plateau phase continues as the strain develops from the yield strain (ε_y) to the hardening strain (ε_h). The yield strain (ε_y) can be calculated by Eq. (10).

$$\varepsilon_y = \frac{N_{0t}}{(EA)_t} \tag{10}$$

In the last phase of the envelope curve, the hardening phase, a quadratic polynomial is used to approximate the strain force curve. The three conditions, shown in Eqs.(11), are considered to determine the three parameters of this quadratic polynomial. The results are shown below in Eqs.(12)

$$F(\varepsilon_h) = N_{0t} \tag{11-a}$$

$$\frac{\partial F}{\partial \varepsilon}|_{\varepsilon=\varepsilon_h} = E_h \tag{11-b}$$

$$\frac{\partial F}{\partial \varepsilon}|_{\varepsilon=\varepsilon_u} = 0 \tag{11-c}$$

$$k_1 = \frac{E_h}{2(\varepsilon_h - \varepsilon_u)} \tag{12-a}$$

$$k_2 = -\frac{E_h \varepsilon_u}{\varepsilon_h - \varepsilon_u} \tag{12-b}$$

$$k_3 = \frac{-\frac{E_h \varepsilon_h^2}{2} + E_h \varepsilon_h \varepsilon_u + P\varepsilon_h - P\varepsilon_u}{\varepsilon_h - \varepsilon_u} \tag{12-c}$$

There are still 3 parameters, $\varepsilon_h, \varepsilon_h\ and\ E_h$, in Eq.(9), that need to be determined in the proposed envelope formula. All the load-strain curves of the specimens under monotonic loading and the load-strain envelope curves of the specimens under repeated loading are used in the regression to determine the these 3 parameters. The final formulas are shown in Eqs.(13).

$$\varepsilon_u = 0.05 \tag{13-a}$$

$$\varepsilon_h = \frac{\varepsilon_u}{-3.5t - 0.05\alpha_{CA} + 56.5} \tag{13-b}$$

$$E_h = \frac{(EA)_t}{2t + 0.1\alpha_{CA} - 1.45} \tag{13-c}$$

4.4.2. Unloading and reloading curves

As depicted in Fig.7, the unloading and reloading curves are nearly linear, and the stiffness, i.e., the slopes, are very close, as illustrated in Fig.12. Furthermore, as discussed in Section 4.3, stiffness degradation was observed during the tests. Consequently, a linear model with progressively decreasing stiffness is employed to characterize the unloading and reloading behavior of the UHPCFST under repeated tension, as presented in Eq. (14), where F_{ul} represents the unloading force, and ε_{ul} denotes the unloading strain, respectively. The reduced section tensile stiffness, $(EA)_t^*$, can be calculated using the original section tensile stiffness,$(EA)_t$, and the stiffness reduction factor (D) introduced in Eq. (7).

$$F = F_{ul} - (EA)_t^*(\varepsilon - \varepsilon_{ul}) \qquad \varepsilon < \varepsilon_{ul} \tag{14-a}$$

$$(EA)_t^* = D(\varepsilon_{ul})(EA)_t \tag{14-b}$$

4.4.3. Evaluation of the proposed strain-force model

Comparisons between the predictions of the proposed empirical strain-force model and the experiment data for the monotonic and repeated tensile experiments tested in this paper are shown in Fig.19. The strain-force model proposed in this study demonstrates a high accuracy in predicting the strain-force curves of the monotonic tensile tests and the skeleton strain-force curves of the repeated tensile tests. Additionally, it also provides accurate predictions to the unloading and reloading paths of the repeated tensile tests.

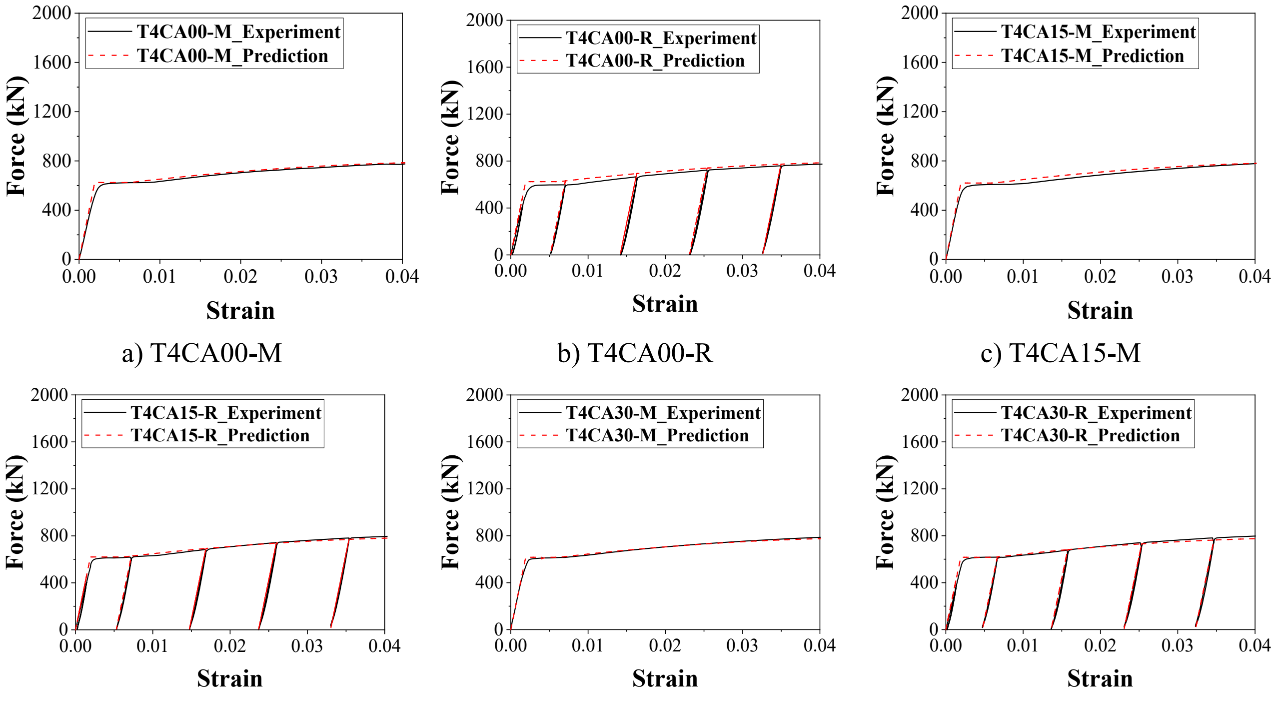

a) T4CA00-M b) T4CA00-R c) T4CA15-M

c) T4CA15-R d) T4CA30-M e) T4CA30-R

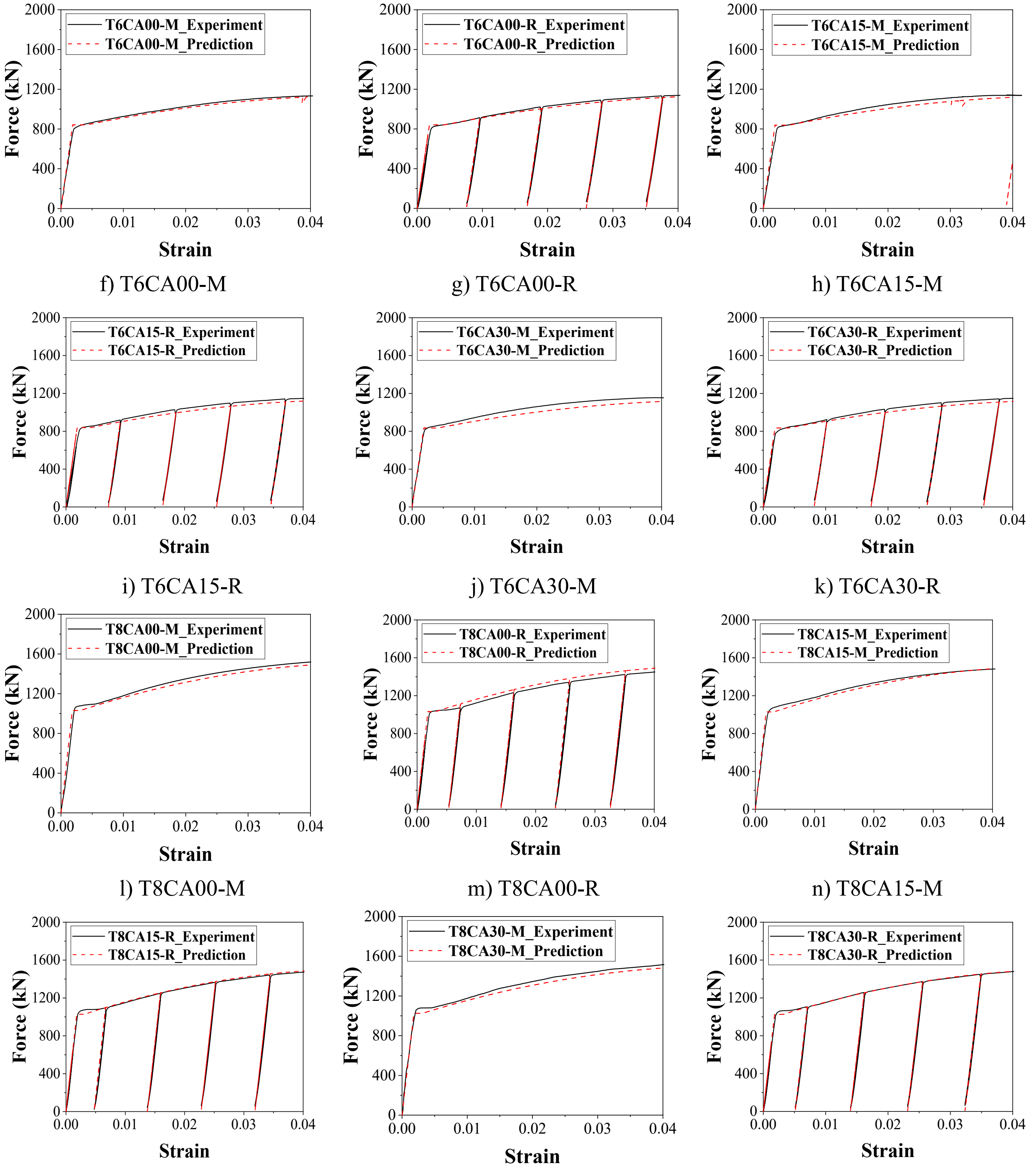

f) T6CA00-M g) T6CA00-R h) T6CA15-M

i) T6CA15-R j) T6CA30-M k) T6CA30-R

l) T8CA00-M m) T8CA00-R n) T8CA15-M

o) T8CA15-R p) T8CA30-M q) T8CA30-R

Fig.19. Prediction of the proposed strain-force model on UHPCFSTs

To verify further the proposed strain-force models, Experimental strain-force curves of CFSTs under tensile loads from Pan and Zhong [17], Han et al.[18], and Lai et al[19] are compared with the predictions of the proposed strain-force model. The details of their tested specimens are presented in

Table.8. It is worth noting that the volume fraction of coarse aggregate (α_{CA}) for these specimens was taken as 0. It should be noted that the four specimens from Pan and Zhong[18] have been re-labeled as PZ-1, PZ-2, PZ-3 and PZ-4, respectively. The other specimens retain their original labels. The definitions of these labels can be found in the corresponding published literatures [17-19].

Table.8 Detail parameters of the CFSTs tests by Pan and Zhong[18], Han et.al[19] , and Lai et.al[21]

No	Ref and Specimen type	Specimen label	D×t× L (mm)	f_y (MPa)	E_s (GPa)	f_t (MPa)	f_t^* (MPa)
1	Pan and Zhong	PZ1	57.8 × 0.8 × 350	277.8	200	2.88	0
2	[18]	PZ2	57.8 × 0.8 × 350	277.8	200	2.88	0
3		PZ3	59 × 1.6 × 350	277.8	200	2.88	0
4	CFST	PZ4	59 × 1.6 × 350	277.8	200	2.88	0
5		sb1-1	140 × 3.8 × 490	342	201	4.03	0
6		sb1-2	140 × 3.8 × 490	342	201	4.03	0
7		fb1-1	140 × 3.8 × 490	342	201	5.85	0.93
8		fb1-2	140 × 3.8 × 490	342	201	5.85	0.93
9		su1-1	140 × 3.8 × 490	342	201	4.03	0
10		su1-2	140 × 3.8 × 490	342	201	4.03	0
11	Han	fu1-1	140 × 3.8 × 490	342	201	5.85	0.93
12	[19]	fu1-2	140 × 3.8 × 490	342	201	5.85	0.93
13		sb2-1	180 × 3.85 × 630	332	209	4.03	0
14	CFST	sb2-2	180 × 3.85 × 630	332	209	4.03	0
15	FRCFST	fb2-1	180 × 3.85 × 630	332	209	5.85	0.93
16		fb2-2	180 × 3.85 × 630	332	209	5.85	0.93
17		su2-1	180 × 3.85 × 630	332	209	4.03	0
18		su2-2	180 × 3.85 × 630	332	209	4.03	0
19		fu2-1	180 × 3.85 × 630	332	209	5.85	0.93
20		fu2-2	180 × 3.85 × 630	332	209	5.85	0.93
21		47.6V2T20	120 × 2.5 × 300	285	199	8.8	2.015
22		47.6V2T60	120 × 2.5 × 300	285	199	9.8	2.015
23	Lai	47.6V2T180	120 × 2.5 × 300	285	199	12	2.015
24	[21]	47.6V2T90	120 × 2.5 × 300	285	199	10.8	2.015
25		34.6V2T90	120 × 3.5 × 300	285	199	10.8	2.015
26	RPCFST	40.0V2T90	120 × 3.0 × 300	285	199	10.8	2.015
27		47.6V3T90	120 × 2.5 × 300	285	199	12.7	3.0225
28		47.6V1T90	120 × 2.5 × 300	285	199	8.3	1.0075
29		47.6V0T90	120 × 2.5 × 300	285	199	4.7	0

In Table.8, CFST, FRCFST and RPCFST denote, respectively, concrete filled steel tube, fiber reinforced concrete filled steel tube and reactive powder concrete filled steel tube; D, t and L denote, respectively, outside diameter, thickness and length of a steel tube; f_y is yield strength of steel; E_s is elastic module of steel; f_t is tensile strength of concrete; f_t^* is residual tensile strength of concrete.

The comparisons are presented in Fig.20. It can be observed that for the CFST and the FRCFST specimens, the proposed model tends to overestimate the force. This can be attributed to the relatively poorer mechanical properties[46,47] of the normal concrete (NC) and the fiber-reinforced concrete (FRC) compared to the ultra-high performance concrete (UHPC). The NC and FRC are more prone to fracture during tension, resulting in a lower force at the same strain level. The reactive powder concrete (RPC) exhibits similar mechanical behavior to the UHPC[48]. Compared to the CFST with the NC, the tensile strength of the UHPC in the UHPCFST should be considered. It is the reason that the proposed empirical model for the UHPCFST overestimates the tensile force of the CFST, but accurately predicts the strain-force curve of the RPCFST.

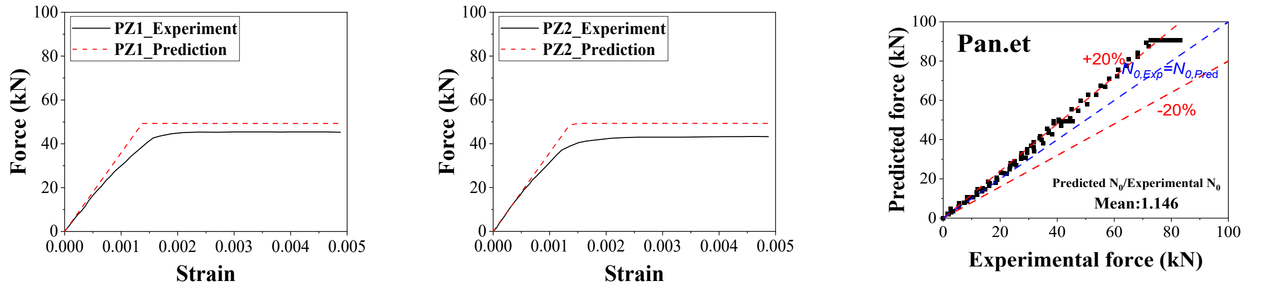

a) PZ1 b) PZ2 c) Evaluation on Pan's all test curves

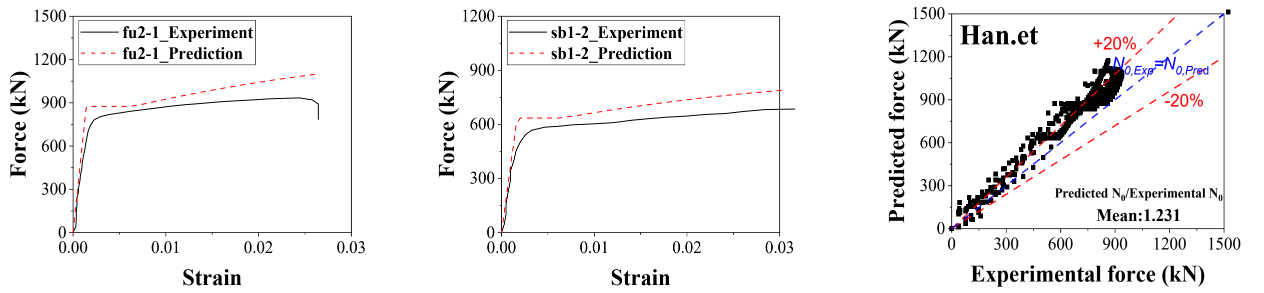

d) fu2-1 e) sb1-1 f) Evaluation on Han's all test curves

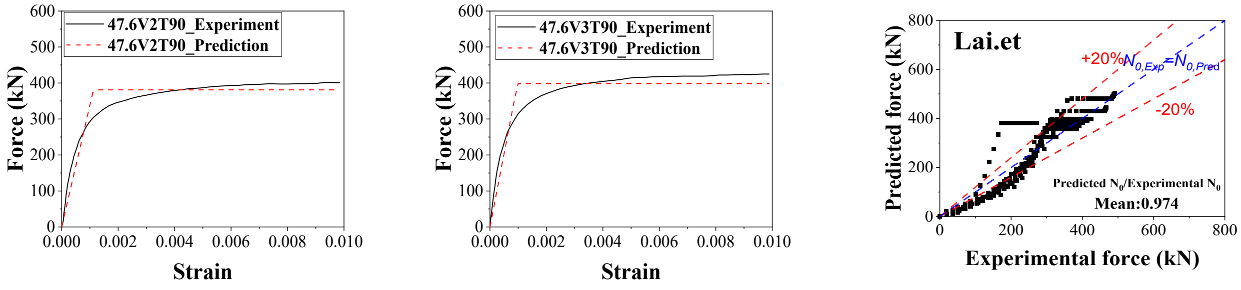

g) 47.6V2T90 h) 47.6V3T90 i) Evaluation on Lai's all test curves

Fig.20. Prediction of proposed strain-force model on CFST tensile strain-force curves collected from published literatures

The above evaluation of the proposed model against the authors' own test results and the results from other researchers also show some limitations of the model. Firstly, the proposed model overestimates the force of CFST with NC. Secondly, the model was developed for the steel tubes with the mechanical properties specified in this paper. Thirdly, the proposed model is only applicable to UHPCFST specimens with a circular cross-section and describes the short-term stress-strain behavior of UHPCFST, because it does not account for concrete shrinkage[49] and potentially creep in the model. Lastly, the model primarily focuses on the tensile aspect of UHPCFST and may not be directly applicable to UHPCFST under reverse cyclic loading. Additional studies on, e.g., opening and closing of concrete cracks, are required when addressing this issue.

5. Conclusion

In the present work, 18 UHPCFST specimens are tested under monotonic and repeated axial tensile load to investigate tensile mechanical performance of the UHPCFST. Based on the results and discussions presented in this paper, the following conclusions can be drawn.

1) All the UHPCFST specimens exhibit the same fracture failure of the outer steel tube at virtually the same location where the UHPC section fractures. Importantly, significant deformation is observed prior to failure, indicating that the tensile failure of the UHPCFST represents a form of ductile failure mode.

2) The tensile strength significantly increases with the increase in steel tube thickness. However, the enhancement effect, as represented by the tensile strength factor (k_t), decreases with the increase of the steel ratio (α). Similarly, the tensile stiffness exhibits a similar tendency to the tensile strength.
3) For UHPCFSTs under axial monotonic and repeated tension with same design factors. The load-strain curves of the UHPCFST under monotonic axial tension are almost identical to the envelopes of the load-strain curves of the UHPCFST under repeated axial tension.
4) The unloading and reloading curves of a UHPCFST under repeated axial tensile load are almost linear. Stiffness degradation occurs, where the tensile section stiffness remains relatively constant before fracturing before a significant decrease thereafter. An exponential decay formula is proposed to predict the degradation.
5) The experimental results are used to evaluate existing formulas from the codes of Europe, USA, and China, as well as from other researchers. The results suggest that Lai's formula offers a reliable prediction to the tensile strength of UHPCFST and Xu's formula can give a good prediction to the tensile stiffness of UHPCFST. The deviations of the predictions from the design codes are larger than those from the formulas developed by the researchers, suggesting that the codes developed for CFST may not be entirely appropriate for designing UHPCFST
6) A simple three-phase empirical model is proposed to describe the load-strain curve of a UHPCFST under tension. Moreover, evaluations of the proposed strain-force model are made through comparisons with the experimental data from published literatures. The proposed model can provide accurate strain-force predictions for UHPCFST/RPCFST, while likely

overestimates the force of CFST/FRCFST. The model can be applied in practical design, analysis, and numerical simulations of UHPCFST.

Acknowledgments

This work was supported by the National Natural Science Foundation of China (Grant Nos. 52178157, 51738011). The last author is grateful to the Royal Society for the financial support (IEC\NSFC\181449).

Reference

[1] Richard P, Cheyrezy M. Composition of reactive powder concretes. Cement and Concrete Research 1995;25:1501–11.

[2] Su Y, Wu C, Li J, Li Z-X, Li W. Development of novel ultra-high performance concrete: From material to structure. Construction and Building Materials 2017;135:517–28.

[3] Yoo D-Y, Banthia N. Mechanical properties of ultra-high-performance fiber-reinforced concrete: A review. Cement and Concrete Composites 2016;73:267–80.

[4] Tam CM, Tam VWY, Ng KM. Assessing drying shrinkage and water permeability of reactive powder concrete produced in Hong Kong. Construction and Building Materials 2012;26:79–89.

[5] Bahmani H, Mostofinejad D. Microstructure of ultra-high-performance concrete (UHPC) – A review study. Journal of Building Engineering 2022;50:104118.

[6] Yu M, Liao W, Liu S, Wang T, Yu C, Cheng S. Axial compressive performance of ultra-high performance concrete-filled steel tube stub columns at different concrete age. Structures 2023;55:664–76.

[7] Wu F, Xu L, Zeng Y, Yu M, Li B. Behavior of CA-UHPC filled circular steel tube stub columns under axial compression. Journal of Constructional Steel Research 2023;211:108204.

[8] Chen D, Wu J, Zha X, Hou X. Study on selection of concrete-filled steel tubular X-column in large-scale

cooling tower. Jianzhu Jiegou Xuebao/Journal of Building Structures 2021;42:322–31.

[9] Chen D, Zha X, Hou X, Zhou G, Li G. Compression behavior of the concrete-filled steel tubular X-column. Jianzhu Jiegou Xuebao/Journal of Building Structures 2021;42:351–60.

[10] Chen D, Zha X, Hou X. Stability performance analysis of concrete-filled steel tubular double cross column in super large-scale cooling tower. Huazhong Keji Daxue Xuebao (Ziran Kexue Ban)/Journal of Huazhong University of Science and Technology (Natural Science Edition) 2022;50:93–8.

[11] Chen D, Zha X, Xu P, Zhai X. Experimental and theoretical investigation of concrete-filled steel tubular x-column under axial compression. Journal of Constructional Steel Research 2020;170.

[12] Chen D, Zha X, Xu P, Li W. Stability of slender concrete-filled steel tubular X-column under axial compression. Journal of Constructional Steel Research 2021;185.

[13] Jani K, Patel PV. Analysis and design of diagrid structural system for high rise steel buildings. vol. 51, 2013, p. 92–100.

[14] Liu C, Li Q, Lu Z, Wu H. A review of the diagrid structural system for tall buildings. Structural Design of Tall and Special Buildings 2018;27.

[15] Zhang C, Zhao F, Liu Y. Diagrid tube structures composed of straight diagonals with gradually varying angles. Struct Design Tall Spec Build 2012;21:283–95.

[16] Zhao F, Zhang C. Diagonal arrangements of diagrid tube structures for preliminary design. Structural Design of Tall and Special Buildings 2015;24:157–75.

[17] Boake TM. Diagrid Structures: Systems, Connections, Details. Walter de Gruyter; 2014.

[18] Pan G, Zhong S. Axial Tensile Constitutive Relationship of Concrete Filled Steel Tube. Industrial Construction 1990:30–7.

[19] Han L-H, He S-H, Liao F-Y. Performance and calculations of concrete filled steel tubes (CFST) under axial

tension. Journal of Constructional Steel Research 2011;67:1699–709.

[20] Xu L-Y, Tao M-X, Zhou M. Analytical model and design formulae of circular CFSTs under axial tension. Journal of Constructional Steel Research 2017;133:214–30.

[21] Lai Z, Yao P, Huang W, Chen B, Ying Z. Reactive powder concrete-filled steel tube (RPCFT) members subjected to axial tension: Experimental study and design. Structures 2020;28:933–42.

[22] Li L, Xu L, Huang L, Xu F, Huang Y, Cui K, et al. Compressive fatigue behaviors of ultra-high performance concrete containing coarse aggregate. Cement and Concrete Composites 2022;128:104425.

[23] Xu L, Wu F, Chi Y, Cheng P, Zeng Y, Chen Q. Effects of coarse aggregate and steel fibre contents on mechanical properties of high performance concrete. Constr Build Mater 2019;206:97–110.

[24] Xiong M-X, Liew JYR, Wang Y-B, Xiong D-X, Lai B-L. Effects of coarse aggregates on physical and mechanical properties of C170/185 ultra-high strength concrete and compressive behaviour of CFST columns. Construction and Building Materials 2020;240:117967.

[25] Han L. Concrete filled steel tubular structures-theory and practice. Science, Beijing; 2007.

[26] Metallic materials -Tensile testing - Part 1: Method of test at room temperature. GB/T 228.1:2010. 2010.

[27] Chinese National Standard, Reactive powder concrete 2015.

[28] Wu F, Xu L, Chi Y, Zeng Y, Deng F, Chen Q. Compressive and flexural properties of ultra-high performance fiber-reinforced cementitious composite: The effect of coarse aggregate. Composite Structures 2020;236:111810.

[29] Xu L, Wu F, Chi Y, Cheng P, Zeng Y, Chen Q. Effects of coarse aggregate and steel fibre contents on mechanical properties of high performance concrete. Construction and Building Materials 2019;206:97–110.

[30] Specification for design of ultra-high performance concrete structures. T/CCPA 35—2022/ T/CBMF 185—2022.

[31] Fundamental characteristics and test method of ultra-high performance concrete. T/CBMF 37-2018 T/CCPA7-2018.

[32] Xu F. Study on Uniaxial Tensile Behavior and Stress-strain Relationship of Ultra-high performance Concrete with Coarse Aggregate. Wuhan University, 2022.

[33] Wang F-C, Xie W-Q, Li B, Han L-H. Experimental study and design of bond behavior in concrete-filled steel tubes (CFST). Engineering Structures 2022;268:114750.

[34] Eurocode 4: Design of composite steel and concrete structures Part 1-1: General rules and rules for buildings

[35] ANSI/AISC 360-16: Specification for Structural Steel Buildings 2016.

[36] CN-GB50936-2014: Technical code for concrete-filled steel tubular structures (press in Chinese) 2014.

[37] Lai Z, Yao P, Huang W, Chen B, Ying Z. Reactive powder concrete-filled steel tube (RPCFT) members subjected to axial tension: Experimental study and design. Structures 2020;28:933–42.

[38] Xu L-Y, Tao M-X, Zhou M. Analytical model and design formulae of circular CFSTs under axial tension. Journal of Constructional Steel Research 2017;133:214–30.

[39] Lai MH, Song W, Ou XL, Chen MT, Wang Q, Ho JCM. A path dependent stress-strain model for concrete-filled-steel-tube column. Engineering Structures 2020;211:110312.

[40] Ho JCM, Ou XL, Chen MT, Wang Q, Lai MH. A path dependent constitutive model for CFFT column. Engineering Structures 2020;210:110367.

[41] Lai MH, Liang YW, Wang Q, Ren FM, Chen MT, Ho JCM. A stress-path dependent stress-strain model for FRP-confined concrete. Engineering Structures 2020;203:109824.

[42] Dong CX, Kwan AKH, Ho JCM. Axial and lateral stress-strain model for concrete-filled steel tubes with FRP jackets. Engineering Structures 2016;126:365–78.

[43] Kwan AKH, Dong CX, Ho JCM. Axial and lateral stress–strain model for concrete-filled steel tubes. Journal

of Constructional Steel Research 2016;122:421–33.
[44] Dong CX, Kwan AKH, Ho JCM. Effects of external confinement on structural performance of concrete-filled steel tubes. Journal of Constructional Steel Research 2017;132:72–82.
[45] Kwan AKH, Dong CX, Ho JCM. Axial and lateral stress–strain model for circular concrete-filled steel tubes with external steel confinement. Engineering Structures 2016;117:528–41.
[46] Bajaber MA, Hakeem IY. UHPC evolution, development, and utilization in construction: a review. Journal of Materials Research and Technology 2021;10:1058–74.
[47] Wang S, Xu L, Yin C, Chen Z, Chi Y. Experimental investigation on the damage behavior of ultra-high performance concrete subjected to cyclic compression. Composite Structures 2021;267.
[48] Du J, Meng W, Khayat KH, Bao Y, Guo P, Lyu Z, et al. New development of ultra-high-performance concrete (UHPC). Composites Part B: Engineering 2021;224:109220.
[49] Lai MH, Binhowimal SAM, Griffith AM, Hanzic L, Wang Q, Chen Z, et al. Shrinkage design model of concrete incorporating wet packing density. Construction and Building Materials 2021;280:122448.